THE ORIGIN OF POLYGONAL TROUGHS IN THE CALORIS BASIN OF MERCURY.

T. R. Watters[1], **F. Nimmo**[2] and **M. S. Robinson**[3], [1]Center for Earth and Planetary Studies, National Air and Space Museum, Smithsonian Institution, Washington, D.C. 20560 (watterst@si.edu); Department of Earth Sciences, University of California Santa Cruz, Santa Cruz, California 95064 (nimmo@ess.ucla.edu); [3]Department of Geological Sciences, Northwestern University, Evanston, Illinois 60208 (robinson@eros.earth.nwu.edu).

Introduction: The Caloris basin is one of the largest impact basins in the solar system with a main rim diameter estimated to be 1300 km [1]. The imaged portion is characterized by smooth plains extensively deformed by basin-concentric and basin-radial wrinkle ridges (Fig. 1a). The wrinkle ridges probably formed in response to basin-interior compression at roughly the same time as wrinkle ridges and lobate scarp thrust faults formed in exterior smooth plains and intercrater plains [2]. Complex extensional troughs crosscut the wrinkle ridges in the Caloris basin and appear to be the youngest endogenic features in the basin. The troughs consist of linear and sinuous segments (Fig. 1b) that range in width from hundreds of meters up to ~10 km [3]. Exposed floors appear to be flat, consistent with the interpretation that the troughs are graben [1, 3]. Troughs are both basin-concentric and basin-radial forming giant polygons [1, 3, 4] up to 40 to 50 km across. Morphologically similar polygonal troughs have been found in the northern lowlands of Mars [5, 6, 7] and in volcanic plains on Venus [8, 9]. However, no analogous landforms occur in the floor materials of impact basins on the Moon or Mars. Below, we argue that the late-stage extension in Caloris is caused by lateral crustal flow into the basin.

Topography and Strain: Topographic profiles derived from photoclinometry indicate the Caloris troughs have relatively flat floors (Fig. 2) and trough walls have gentle slopes ranging from 4º to 6º, not exceeding 10º (n = 7). The depth of the measured troughs varies from ~100 m up to a maximum of ~220 m. The topographic data indicate that many troughs are flanked on both sides by gently sloping rises (Fig. 2), similar to martian polygonal troughs [10].

The extensional strain reflected by the polygonal troughs can be estimated using the displacement-length (*D-L*) ratio γ of the trough-forming graben and the dips of the normal faults [11]. Assuming initial fault plane dips characteristic of normal faults (~60°), estimates of the displacement on the normal faults range from 0.11 to 0.25 km with an average of ~0.2 km (n = 7). A linear fit to the *D-L* data for the troughs yields a value of γ ~2.2×10^{-3} (θ = 60°). Determination of γ is complicated by the variability of the trough width and the combination of highly sinuous and linear trough segments. Preliminary estimates of the extensional strain over the total area of the imaged portion of the Caloris basin is ~0.05%, equivalent to an elastic stress of ~50 MPa.

Lateral Crustal Flow Model: We assume that the initial basin was partially filled with lavas, resulting in early subsidence and compression. However, the crust beneath the basin was probably still thinner than the surrounding crust. The resulting lateral crustal thickness contrasts give rise to lateral pressure gradients which can drive flow towards the basin center, even if the basin is isostatically compensated [12]. This lateral flow will result in late-stage uplift of the existing basin materials (Fig. 3a) at a rate determined by crustal thickness, rheology, and thermal gradient.

The evolution of the topography of a Caloris-sized impact basin was simulated over a 500 Myr period (Fig. 3b). The initial basin shape is assumed to be flat-floored, in agreement with recent studies of gravity anomalies associated with lunar mascons [13]. The evolution of the basin topography was calculated with the lower crustal flow model [12], using a temperature- and stress-dependent dry plagioclase rheology and a crustal thickness (120 km) and heat flux (23.7 mWm^{-2}) consistent with previous estimates [14, 15]. For the initial basin geometry assumed, the surface extensional stresses reach a peak value of 100 MPa at about 300 km inwards of the basin rim (Fig. 3b). Both the predicted location and the magnitude of the stresses arising from lateral crustal flow are compatible with the observations of the Caloris polygonal troughs. An initially Gaussian basin shape results in similar stress magnitudes, but with peak stresses at the basin center.

The degree of relaxation depends on the crustal thickness, rheology and heat flux [12]. Using the assumed dry plagioclase rheology, the degree of relaxation as a function of heat flux and crustal thickness is shown in Fig. 3c. Assuming the heat flux in Mercury is due to radiogenic elements present in the same concentrations as the bulk silicate Earth (BSE), the inferred crustal thickness is in the range of 90 to 140 km for the assumed rheology. This thickness is compatible with previous estimates of 100 to 300 km [14, 15].

The modeling suggests that the absence of extensional troughs in the floors of basins on the Moon and Mars may be due to their generally smaller crustal thickness (Fig. 3c). The relatively thick crust and lack of subsequent geologic activity that allowed the polygonal troughs in the Caloris basin to survive may be unique to Mercury.

References: [1] Strom R. G., Trask N.J. and Guest J.E. (1975) *J. Geophys. Res., 80*, 2478-2507. [2] Watters T.R., Robinson M.S., Bina C.R. and Spudis P.D. (2004) *Geophys. Res. Letts., 31*, L04701. [3] Dzurisin D. (1978) *J. Geophys. Res., 83*, 4883-4906. [4] Melosh H.J. and Dzurisin D. (1978) *Icarus, 35*, 227-236. [5] Carr, 1976 [6] Pechmann J.C. (1980) *Icarus, 42*, 185-210. [7] McGill G.E. (1986) *Geophys. Res. Letts., 13*, 705-708. [8] Johnson C.L. and Sandwell D.T. (1992) *J. Geophys. Res., 97*, 13601-13610. [9] Smrekar S.E. Moreels, P. and Franklin B.J. (2002) *J. Geophys. Res., 107*, 5098. [10] Hiesinger H. and Head J.W. (2000) *J. Geophys. Res., 105*, 11999-12022. [11] Cowie P.A. Scholz C.H. Edwards M. and Malinverno, A. (1993) *J. Geophys. Res., 98*, 17911-17920. [12] Nimmo, F. and Stevenson D.J. (2001) *J. Geophys. Res., 106*, 5085-5098. [13] Watters T.R., and Konopliv A.S. (2001) *Planet. Space Sci., 49*, 743-748. [14] Anderson J.D. Jurgens R.F. Lau E.L., and Slade M.A. (1996) *Icarus, 124*, 690-697. [15] Nimmo F. and Watters T.R. (2004) *Geophys. Res. Letts., 31*, L02701.

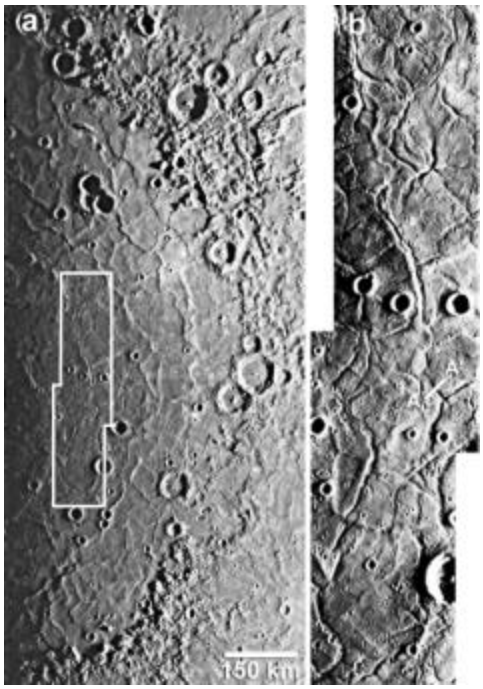

Figure 1. Polygonal troughs in the Caloris basin. a) The interior plains of the Caloris basin show evidence of compressional (wrinkle ridges) and extensional (troughs) deformation. b) High resolution image mosaic of a portion of the interior plains showing extensional troughs that form giant polygons (Mariner 10 images 0529055 and 0529056, the maximum width of the mosaic is ~115 km).

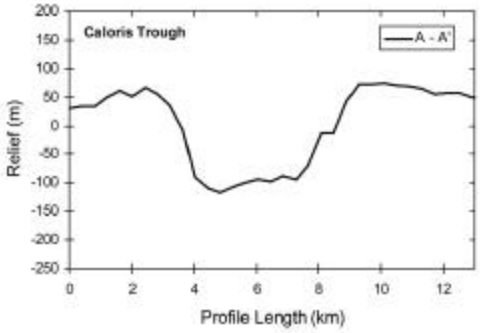

Figure 2. Topographic profile across a trough in the Caloris basins. The Caloris trough has relatively flat floor, gently sloping walls, and raised or rounded rims. Profile location is shown in Fig. 1b. Elevations are relative to an arbitrary datum (vertical exaggeration ~20:1).

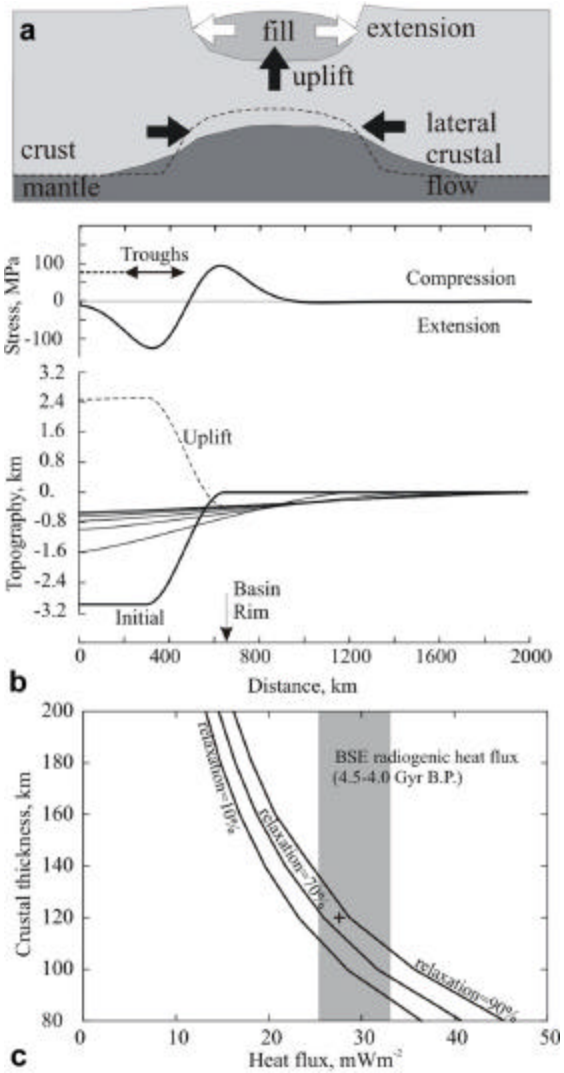

Figure 3. Lateral crustal flow model. a) Schematic of the effect of lateral crustal flow on basin topography. Initial base of crust indicated by dotted line. b) Model of lower crustal flow. Bold line in lower panel (b) outlines pan-shaped initial isostatically compensated basin topography; thin lines detail evolution of topography at 5, 34, 96, 210, 350 and 500 Myr; dashed line shows total (isostatic) uplift. Upper panel (b) shows radial stresses caused by uplift, assuming an elastic thickness of 50 km and Young's modulus of 100 GPa. Location of polygonal troughs imaged in Caloris denoted by horizontal arrow; dashed line denotes poorly or unimaged area. c) Degree of basin relaxation (ratio of initial basin depth to central uplift) as a function of heat flux and crustal thickness after 500 Myr. Shaded region denotes radiogenic heat flux on Mercury assuming bulk silicate Earth (BSE) concentrations; cross denotes model shown in Fig 3b.